Imaging of labile Fe2+ and Fe3+ in living Arabidopsis thaliana roots

Carine Alcon, Arnaud Comte, Catherine Curie, Tou Cheu Xiong

Imaging of labile Fe^{2+} and Fe^{3+} in living *Arabidopsis thaliana* roots

Corresponding author: Tou Cheu Xiong (tou-cheu.xiong@inrae.fr).

Dear Editor,

Imaging of iron (Fe) in living organisms is challenging and ways to visualize Fe are limited to sophisticated elemental methods and/or fixed tissues. As a transition metal, Fe cycles between two oxidation states, Fe^{2+} and Fe^{3+}, losing or donating an electron in doing so. This property enables Fe to participate in key metabolic pathways (Briat et al., 2015). Imaging of the redox species of Fe is therefore of interest to decipher its biological functions. Cellular Fe is partitioned into two distinct pools (Koppenol and Hider, 2019): static Fe, which is tightly bound to its ligands, and labile Fe, which is weakly bound and can be exchanged between ligands rather effortlessly. To date, there are no reports describing the distribution of Fe^{2+} and Fe^{3+} labile pools in living organisms. The Perls-DAB histochemical method stains Fe in fixed tissues, chiefly the Fe^{3+} form (Roschzttardtz et al., 2009), but it mainly detects the static Fe fraction since labile Fe is likely lost during tissue fixation. In order to address the dynamics of Fe^{2+} and Fe^{3+} labile pools in live plants, we have established a method combining two probes, which enables specific detection of the redox state of the labile Fe pools.

To that aim we have selected two fluorescent probes, SiRhoNox-1 (Hirayama et al., 2017) and MPNBD (Park et al., 2014), which we used to image labile Fe^{2+} and Fe^{3+}, respectively, in Arabidopsis (*Arabidopsis thaliana*) roots (Supplemental Methods). The two probes were chosen in such a way that their spectral properties do not overlap, allowing their simultaneous utilization without any crosstalk (Supplemental Figure S1). The specificity of each probe was reconfirmed *in vitro* albeit in an aqueous buffer adapted for plant applications (Supplemental Figure S2). The fluorescence of the two probes, though depending on pH, was found rather stable at physiological pH (6.0-6.5) (Supplemental Figure S2G,H). Fluorescence intensity fluctuations must therefore be interpreted cautiously. The selectivity of the probes toward the redox state of Fe was tested by applying them to various Fe species *in vitro*. The mixed probes

detected labile Fe species (Fe(II)-acetate, Fe(II)-SO_4, Fe(III)-NO_3, Fe(III)-Cl_3), but not the Fe species involved in strong chelates such as EDTA or citrate (Fig. 1A). *In vitro* ascorbate-mediated reduction of Fe^{3+} species into Fe^{2+} was successfully monitored by the probes (Fig. 1B), suggesting that the method is suitable to assess reductase activity *in vivo*.

SiRhoNox-1 and MPNBD were applied in combination to 7 day-old plants and compared with Perls-DAB staining (Fig. 1C-K). The fluorescent signals observed with the two probes were heterogeneously distributed along the entire primary root and were distinct from each other (Supplemental Figure S3). Three root zones representative of the distribution of Fe^{2+} and Fe^{3+} were observed at higher magnification (Fig. 1D,G and J). Fe^{3+} was markedly predominant in the primary root apex (Fig. 1J) but absent in the young lateral root (Supplemental Figure S4A-C). Likewise, Perls-DAB did not stain the emerging root, suggesting that if Fe is present at this stage, its level is under the detection threshold of the two methods (Supplemental Figure S4D). The primary root apex exhibited no Fe^{2+} signal (Fig. 1J). In contrast, in the differentiation zone, a strong Fe^{2+} fluorescent signal was observed at the cell periphery (Fig. 1G), suggesting an apoplastic localization. This observation is in agreement with previous studies reporting elemental analyses of cellular fractions (Bienfait et al., 1985; Ye et al., 2015; Liu et al., 2023). Plasmolysis of root cells confirmed the apoplastic localization of Fe^{2+} (Supplemental Figure S5). Moreover, colocalization of FM4-64 and SiRhoNox-1 revealed the presence of Fe^{2+} at the plasma membrane (Supplemental Figure S5F). 3D images of each root zone emphasized the variation of distribution of the two Fe redox species between cell layers and according to root age (Supplemental Figure S6).

The Fe redox imaging method was applied to the Fe homeostasis ferric reduction oxidase 2 mutant (*fro2)*, the Fe^{3+}/ Fe^{2+} ratio of which is imbalanced owing to a loss of its ability to reduce Fe^{3+} at the root surface (Robinson et al., 1999; Connolly et al., 2003). Compared to wild-type, the differentiation and mature zones of the *fro2* root expectedly exhibited a dramatic decrease of fluorescence with SiRhoNox-1, confirming the specificity of the SiRhoNox-1 probe for Fe^{2+} *in vivo* (Fig. 1E,H, Supplemental Figure S7). The penetration ability of the probes was examined using confocal microscopy. Fluorescence of SiRhoNox-1 and MPNBD was visible in most layers of the root including the vascular cylinder (Fig. 2A-E), indicating that the two probes are able to penetrate all the tissues of the root. In addition, fluorescence signals of the Fe probes were detected inside the cells, showing the permeability of the plasma membrane toward these probes. In epidermal cells, MPNBD fluorescence filled the symplast (Fig. 2F,H), whereas SiRhoNox-1 fluorescence surrounded the cells (Fig. 2G). Upon Fe limitation, SiRhoNox-1 produced intracellular punctuate signals (Fig. 2I,J)(Hirayama et al., 2013; 2017).

Interestingly the method highlighted a polarized pattern of Fe^{2+} at the external side of epidermal cells in the differentiation zone (Fig. 2K-M), a feature that had not been reported previously. Such Fe^{2+} polarization is reminiscent of the polar localization of FRO2 in the same cell type (Martín-Barranco et al., 2020). Remarkably, this polar distribution shifted to the inner side of the epidermal cells in the mature zone (Fig. 2, compare K-O and P-T) where Fe^{2+} was observed in the apoplast (Fig. 2T, red arrows). Quantification of the fluorescence signals allowed detecting subtle changes in the balance between Fe states, as shown in Fe-sufficient and Fe-deficient conditions in wild-type and the *fro2* mutant (Supplemental Figure S7).

In summary, combining fluorescent probes for Fe^{2+} and Fe^{3+} represents an original method to distinguish the redox species of Fe within live tissues, reveals their distribution in root , and uncovers a remarkable polarization of Fe^{2+}. Because this method can detect subtle differences of Fe charges in the tissues, it will become useful to characterize actors of the redox status of Fe, such as oxido-reductases, hence equipping the community with a powerful tool to explore Fe homeostasis in plants.

SUPPLEMENTARY DATA

Supplementary Figure S1. Excitation and emission spectra of SiRhoNox-1 and MPNBD probes at pH 6.0.

Supplementary Figure S2. *In vitro* characterization of the Fe redox SiRhoNox-1 and MPNBD fluorescent probes.

Supplementary Figure S3. Distribution of Fe along the primary root of *A. thaliana* grown on 0.5xMS containing 50 µM Fe-EDTA.

Supplementary Figure S4. The lateral root apex is not stained by the two Fe probes.

Supplementary Figure S5. Fe is localized in the apoplastic space of root epidermal cells.

Supplementary Figure S6. Differential spatial distribution of Fe^{2+} and Fe^{3+} according to the developmental stage of the root in 7 day-old plants grown in Fe replete conditions.

Supplementary Figure S7. Changes in Fe redox state are dependent on growth conditions and Fe homeostasis.

Supplementary Methods.

FUNDING

This work was supported by the INRAE BAP 2020 grant “FluoMet” and the CNRS-MITI Metallomix 2021 grant “DesciFer”.

ACKNOWLEDGMENTS

We acknowledge the MRI imaging facility, member of the France-BioImaging national infrastructure supported by the French National Research Agency (ANR-10-INBS-04, «Investments for the future»)" and PHIV-La Gaillarde facility.

Carine Alcon[1], Arnaud Comte[2], Catherine Curie[1], Tou Cheu Xiong[1]

[1] IPSiM, Univ Montpellier, CNRS, INRAE, Montpellier, France,

[2] Institut de Chimie et de Biochimie Moléculaires et Supramoléculaires, Lyon, France

The author responsible for distribution of materials integral to the findings presented in this article in accordance with the policy described in the Instructions for Authors (https://academic.oup.com/plphys/pages/General-Instructions) is Tou Cheu Xiong (tou-cheu.xiong@inrae.fr).

AUTHOR CONTRIBUTIONS

CA and TCX performed fluorescence imaging and Perls-DAB staining, designed and carried out the experiments; AC performed fluorescent probe synthesis; CA, TCX, CC wrote the paper.

Figure 1: *In vitro and in vivo* detection of labile Fe^{2+} and Fe^{3+} using fluorescent probes. **(A,B)** Determination of the specificity of the SiRhoNox-1 and MPNBD probes *in vitro*. (**A**) Both probes were applied in combination to 1 mM solutions of a variety of Fe species. (**B**) Reduction of Fe^{3+} by addition of 1mM ascorbate (ASC) to the different Fe species allowed detecting a change of Fe redox state. (**C-K**) *In vivo* imaging of Fe in the roots of 7 day-old Arabidopsis plants grown on 0.5xMS containing 50µM Fe-EDTA. Labile Fe, detected using combined SiRhoNox-1 and MPNBD (**D, E, G, H, J, K**), was compared with Fe histochemical staining with the Perls-DAB method (**C, F, I**). In the primary root, the mature zone (**C-E)**, differentiation zone (**F-H**) and apex zone (**I-K**) are shown. The projection of maximum intensity of the Z-stack of fluorescent pictures is shown for SiRhoNox-1 (Fe^{2+}, magenta) and MPNBD (Fe^{3+}, green) in wild-type (WT) plants (**D**, **G**, **J**) and in the *fro2* mutant (**E**, **H, K**). Data shown are mean ± SD. Data were collected from 3-4 independent experiments. EDTA= Ethylenediaminetetraacetic acid; a.u.= arbitrary unit; DAB= 3,3'-Diaminobenzidine. All scale bars = 200 µm.

Figure 2: Distribution of labile Fe in the different cell layers of the primary root of *Arabidopsis thaliana*. Images were taken from 7 day-old seedlings. **(A-E)** Representative orthogonal view of the mature zone of the primary root stained with MPNBD (Fe^{3+}, **A**), SiRhoNox-1 (Fe^{2+}, **B**), propidium iodide (Cell wall, **C**), or a merged image of the 3 probes (**D, E**). Labile Fe^{2+} and Fe^{3+} are present in most cell types with a signal in the endodermis. An enlarged view of the endodermal layer indicated by a dashed square shows interruption of the apoplastic fluorescent signal at the Casparian strip (arrowheads, **E**). (**F-J**): MPNBD and SiRhoNox-1 fluorescent signals in root epidermis showing the presence of Fe^{3+} inside the cell (**F**) and Fe^{2+} in the apoplast (**G**) of Fe-replete plants as well as in intracellular dot-like structures of Fe-deficient plants (**H-J**). (**J**) Close-up view of the Fe^{2+} dots presented in (**I**). (**K-T**): Polar distribution of Fe^{2+} in the epidermal cell wall. Differentiation (**K-O**) and mature (**P-T**) zones of the primary root were observed in longitudinal sections. Higher magnification of the epidermal cells (**L**, **Q**) shows polar localization of Fe^{2+}, albeit in opposite pattern in the two zones, which is confirmed by the line profile of the fluorescence intensity of the probes (**M**, **R**). (**N, S, O, T**): Orthogonal view of the differentiation (**N, O**) and mature (**S, T**) root zones, including the corresponding enlarged views (**O, T)** indicated by dashed areas within panels **N** and **S**. (**T**) SiRhoNox-1 labels the intercellular space in the mature zone (red arrows). (**A-G** and **K-T**): Seedlings were grown on 0.5xMS containing 50 µM Fe-EDTA (+Fe). (**H-J**): Seedlings were grown on 0.5xMS without Fe (-Fe). Magenta LUT: SiRhoNox-1; Green LUT: MPNBD; BIOP-Azure LUT: Propidium iodide. MPNBD = 7-(4-methylpiperazin-1-yl)-4-nitrobenzo-2-oxa-1,3-diazole; a.u.= arbitrary unit; EDTA = Ethylenediaminetetraacetic acid; All scale bars = 20 µm.

REFERENCES

Bienfait HF, Van Den Briel W, Mesland-Mul NT (1985) Free Space Iron Pools in Roots: Generation and Mobilization. Plant Physiol **78**: 596–600

Briat J-F, Dubos C, Gaymard F (2015) Iron nutrition, biomass production, and plant product quality. Trends Plant Sci **20**: 33–40

Connolly EL, Campbell NH, Grotz N, Prichard CL, Guerinot ML (2003) Overexpression of the FRO2 Ferric Chelate Reductase Confers Tolerance to Growth on Low Iron and Uncovers Posttranscriptional Control. Plant Physiol **133**: 1102–1110

Hirayama T, Okuda K, Nagasawa H (2013) A highly selective turn-on fluorescent probe for iron(ii) to visualize labile iron in living cells. Chem Sci **4**: 1250

Hirayama T, Tsuboi H, Niwa M, Miki A, Kadota S, Ikeshita Y, Okuda K, Nagasawa H (2017) A universal fluorogenic switch for Fe(II) ion based on N-oxide chemistry permits the visualization of intracellular redox equilibrium shift towards labile iron in hypoxic tumor cells. Chem Sci **8**: 4858–4866

Koppenol WH, Hider RH (2019) Iron and redox cycling. Do's and don'ts. Free Radic Biol Med **133**: 3–10

Liu XX, Zhu XF, Xue DW, Zheng SJ, Jin CW (2023) Beyond iron-storage pool: functions of plant apoplastic iron during stress. Trends Plant Sci **28**: 941–954

Martín-Barranco A, Spielmann J, Dubeaux G, Vert G, Zelazny E (2020) Dynamic Control of the High-Affinity Iron Uptake Complex in Root Epidermal Cells. Plant Physiol **184**: 1236–1250

Park M-J, Jung H-S, Kim Y-J, Kwon Y-J, Lee J-K, Park C-M (2014) High-sensitivity fluorescence imaging of iron in plant tissues. Chem Commun **50**: 8547–8549

Robinson NJ, Procter CM, Connolly EL, Guerinot ML (1999) A ferric-chelate reductase for iron uptake from soils. Nature **397**: 694–697

Roschzttardtz H, Conéjéro G, Curie C, Mari S (2009) Identification of the Endodermal Vacuole as the Iron Storage Compartment in the Arabidopsis Embryo. Plant Physiol **151**: 1329–1338

Schindelin J, Arganda-Carreras I, Frise E, Kaynig V, Longair M, Pietzsch T, Preibisch S, Rueden C, Saalfeld S, Schmid B, et al (2012) Fiji: an open-source platform for biological-image analysis. Nat Methods **9**: 676–682

Ye YQ, Jin CW, Fan SK, Mao QQ, Sun CL, Yu Y, Lin XY (2015) Elevation of NO production increases Fe immobilization in the Fe-deficiency roots apoplast by decreasing pectin methylation of cell wall. Sci Rep **5**: 10746

COMPETING FINANCIAL INTERESTS

The authors declare no competing financial interests.

Figure 1

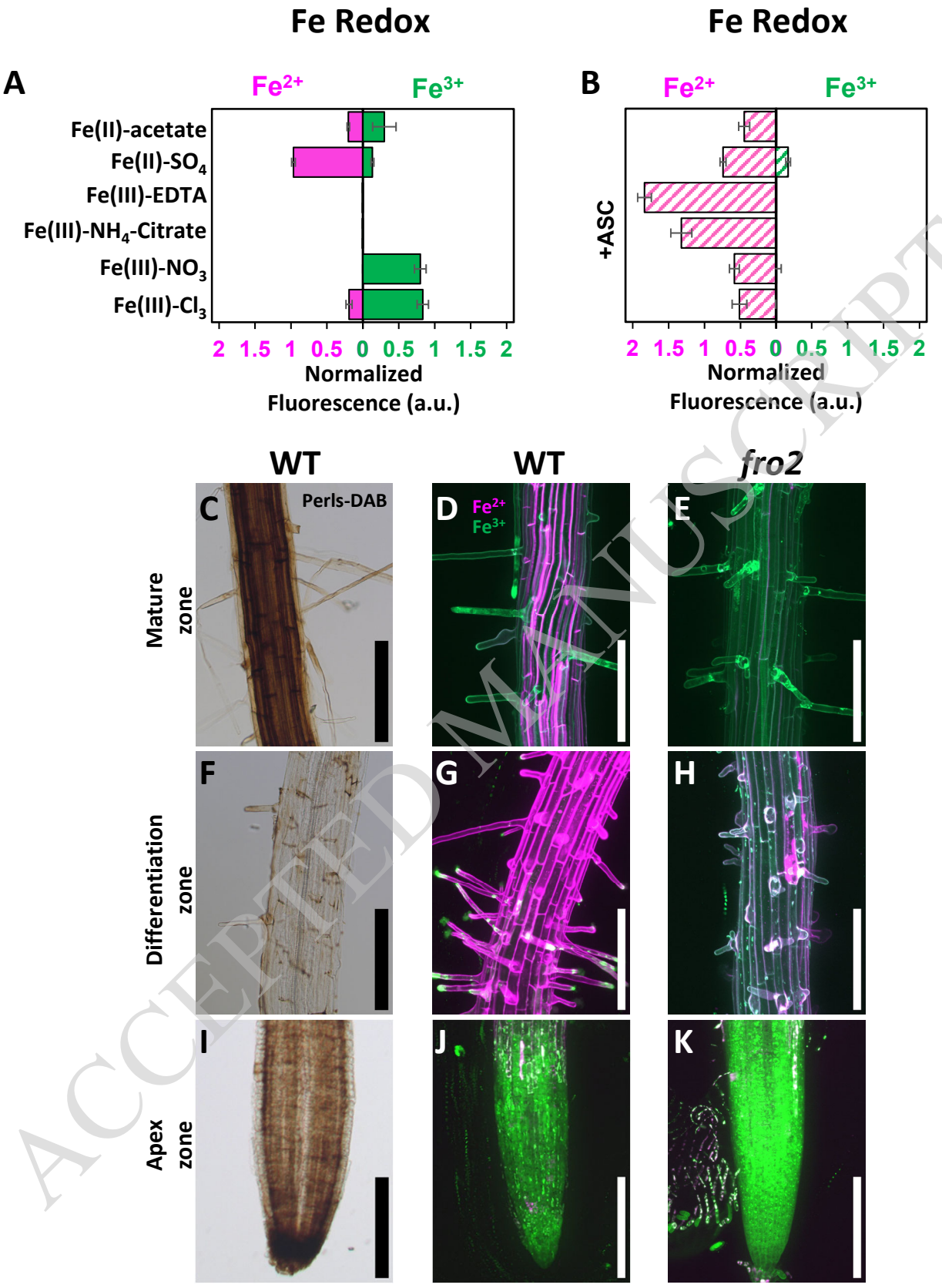

Figure 2

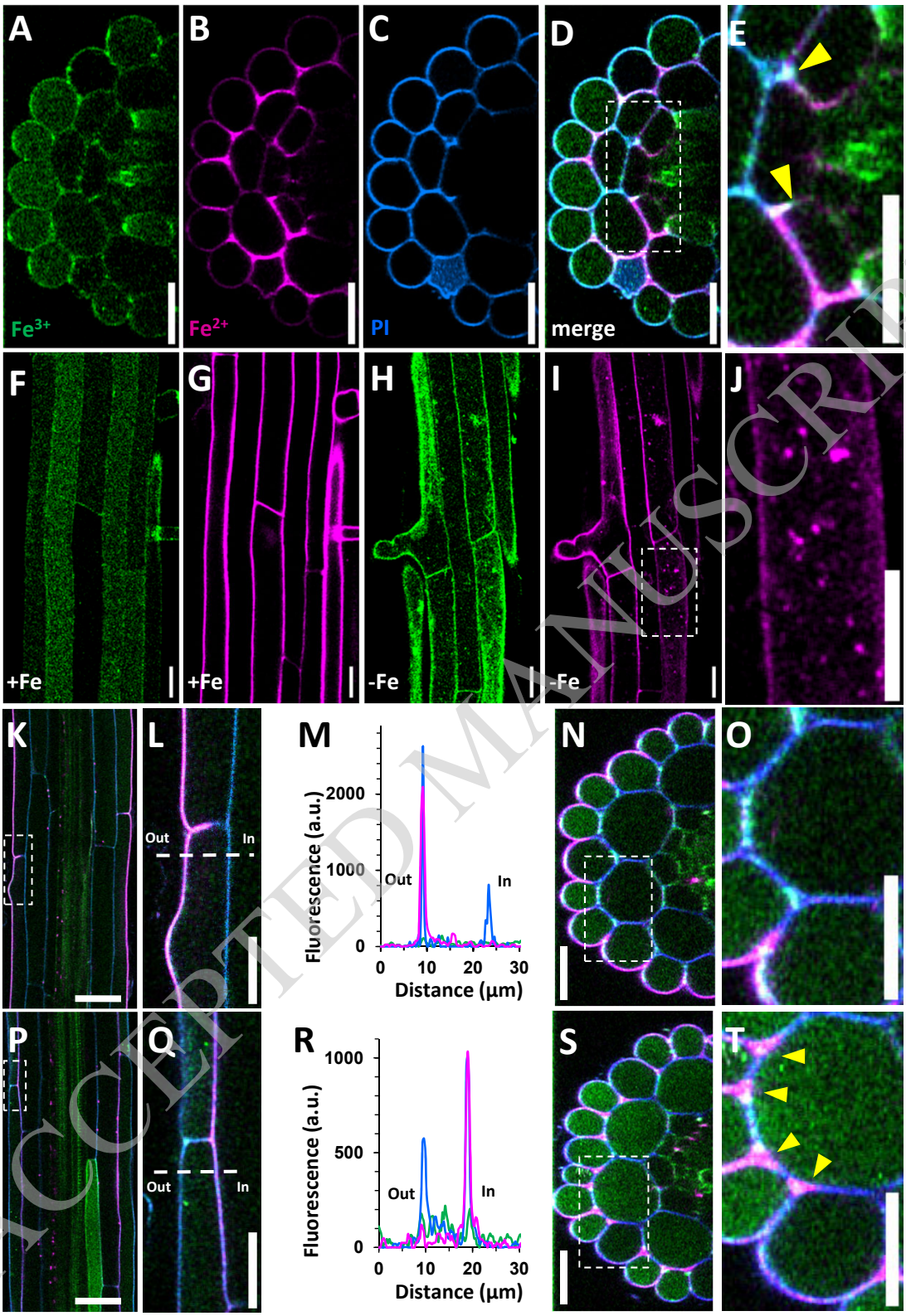

Parsed Citations

Bienfait HF, Van Den Briel W, Mesland-Mul NT (1985) Free Space Iron Pools in Roots: Generation and Mobilization. Plant Physiol 78: 596–600
Google Scholar: Author Only Title Only Author and Title

Briat J-F, Dubos C, Gaymard F (2015) Iron nutrition, biomass production, and plant product quality. Trends Plant Sci 20: 33–40
Google Scholar: Author Only Title Only Author and Title

Connolly EL, Campbell NH, Grotz N, Prichard CL, Guerinot ML (2003) Overexpression of the FRO2 Ferric Chelate Reductase Confers Tolerance to Growth on Low Iron and Uncovers Posttranscriptional Control. Plant Physiol 133: 1102–1110
Google Scholar: Author Only Title Only Author and Title

Hirayama T, Okuda K, Nagasawa H (2013) A highly selective turn-on fluorescent probe for iron(ii) to visualize labile iron in living cells. Chem Sci 4: 1250
Google Scholar: Author Only Title Only Author and Title

Hirayama T, Tsuboi H, Niwa M, Miki A, Kadota S, Ikeshita Y, Okuda K, Nagasawa H (2017) A universal fluorogenic switch for Fe(ii) ion based on N-oxide chemistry permits the visualization of intracellular redox equilibrium shift towards labile iron in hypoxic tumor cells. Chem Sci 8: 4858–4866
Google Scholar: Author Only Title Only Author and Title

Koppenol WH, Hider RH (2019) Iron and redox cycling. Do's and don'ts. Free Radic Biol Med 133: 3–10
Google Scholar: Author Only Title Only Author and Title

Liu XX, Zhu XF, Xue DW, Zheng SJ, Jin CW (2023) Beyond iron-storage pool: functions of plant apoplastic iron during stress. Trends Plant Sci 28: 941–954
Google Scholar: Author Only Title Only Author and Title

Martín-Barranco A, Spielmann J, Dubeaux G, Vert G, Zelazny E (2020) Dynamic Control of the High-Affinity Iron Uptake Complex in Root Epidermal Cells. Plant Physiol 184: 1236–1250
Google Scholar: Author Only Title Only Author and Title

Park M-J, Jung H-S, Kim Y-J, Kwon Y-J, Lee J-K, Park C-M (2014) High-sensitivity fluorescence imaging of iron in plant tissues. Chem Commun 50: 8547–8549
Google Scholar: Author Only Title Only Author and Title

Robinson NJ, Procter CM, Connolly EL, Guerinot ML (1999) A ferric-chelate reductase for iron uptake from soils. Nature 397: 694–697
Google Scholar: Author Only Title Only Author and Title

Roschzttardtz H, Conéjéro G, Curie C, Mari S (2009) Identification of the Endodermal Vacuole as the Iron Storage Compartment in the Arabidopsis Embryo. Plant Physiol 151: 1329–1338
Google Scholar: Author Only Title Only Author and Title

Schindelin J, Arganda-Carreras I, Frise E, Kaynig V, Longair M, Pietzsch T, Preibisch S, Rueden C, Saalfeld S, Schmid B, et al (2012) Fiji: an open-source platform for biological-image analysis. Nat Methods 9: 676–682
Google Scholar: Author Only Title Only Author and Title

Ye YQ, Jin CW, Fan SK, Mao QQ, Sun CL, Yu Y, Lin XY (2015) Elevation of NO production increases Fe immobilization in the Fe-deficiency roots apoplast by decreasing pectin methylation of cell wall. Sci Rep 5: 10746
Google Scholar: Author Only Title Only Author and Title

COMPETING FINANCIAL INTERESTS

The authors declare no competing financial interests.